A Two-step Methodology for Cable Force Identification

Songhan Zhang[a,*], Ruili Shen[b], Yuan Wang[b], Guido De Roeck[c], Geert Lombaert[c], Kaoshan Dai[a]

[a] *Department of Civil Engineering, Sichuan University, China*
[b] *School of Civil Engineering, Southwest Jiaotong University, China*
[c] *Department of Civil Engineering, KU Leuven, Belgium*

Abstract

Vibration-based force identification of cables has been studied for several decades. Most of this work relies on the natural frequencies of the cable for an estimation of the cable force. However, these natural frequencies are also affected by bending stiffness, sag effect and boundary conditions. In the present work, a two-step methodology is developed that allows taking into consideration these effects in the force identification. First, a segment of the cable is considered which is sufficiently short for the sag effect to be negligible. The axial force in this segment is estimated by fitting the measured response to the analytical solution for the transverse motion of the cable in the frequency domain. In this procedure, the bending stiffness is updated exploiting the fact that the estimated axial force should not depend on the frequency, while the boundary conditions do not need to be known. Next, an analytical solution of the static state of the entire cable is derived, taking into account the sag effect, bending stiffness and boundary conditions. The parameters of the entire cable model can then be updated, using the estimated value of the axis force at the location of the segment. Finally, the updated analytical model of the entire cable allows evaluating internal forces such as the cable force and bending moment, as required for estimating the stresses in the cable considering bending deformation. The feasibility of the proposed methodology is verified by means of numerical simulations considering measurement noise and an inaccurate initial guess of the bending stiffness, proving its potential for the health monitoring of cable structures.

Keywords: cable force; parameter estimation; numerical stability; bending stiffness; model updating

1. Introduction

Cables are critical load transferring components in many flexible structures [1]. For the structural health monitoring (SHM) of in-service cable structures, it is important to identify the changes of cable forces which affect the behavior of main structure [2, 3]. During the past decades, vibration-based methods [4, 5] have been extensively studied, as these can be used in operational conditions [6], avoiding, for example, interruption of traffic on bridges [7]. Among the first techniques proposed for cable force identification are those based on the well-known taut string equation [8], considering neither the bending stiffness nor the sag effect. When taking into account the bending stiffness, the dynamic characteristics of the cable become more complicated, however, in particular when accounting for the unknown stiffness of the anchors at the cable ends. Only for the case of hinged-hinged boundary conditions, the cable force can be expressed in closed form as a function of natural frequency [9]. Due to the effect of bending stiffness, the natural frequencies are no longer linearly proportional to the mode order. This effect can be exploited for estimating the bending stiffness when multiple natural frequencies are measured [10]. For the ease of practical application, Ren [11] proposed two empirical equations for estimating the cable force, which respectively consider the sag effect and the bending stiffness, based on fixed-fixed boundary conditions. However, for most real cables acting

*Corresponding author
Email address: songhan.zhang@scu.edu.cn (Songhan Zhang)

as load-carrying members in structures, the boundary conditions are neither hinged-hinged nor fixed-fixed, and the effective length of the cable is usually difficult to determine for the actual anchors at both ends. In addition, the cable force is not constant along the cable, but depending on the position, especially for long cables exhibiting sag. For these reasons, errors are inevitable when applying the above classical methods for identifying the cable force. In order to avoid the difficulties resulting from the boundary conditions and the sag effect, a new method was proposed which considers a cable segment located between the modal nodes of the cable where the transverse displacements are zero [12]. The boundary conditions of such segment can be represented by perfect hinge supports supplemented by rotational springs, while the sag effect can be disregarded as long as the cable segment is sufficiently short. Based on this, the relation between the cable force and natural frequencies was derived, allowing the estimation of the cable force without requiring accurate knowledge of the anchoring stiffness at the cable ends. However, the accurate locations of the modal nodes are difficult to identify without a dense measurement grid, and the stiffnesses of the virtual rotational springs appear as additional unknowns.

As is well known, the transverse motion of the cable is governed by a partial differential equation, and its frequency-domain solution can be expressed as the superposition of a limited number of exponential terms, with coefficients determined by the boundary conditions [13]. Note that these coefficients can as well be determined by fitting this solution to the cable response provided it is measured at a sufficient number of points. The physical parameters can be determined next by searching the minimum of the fitting residual. This concept was originally proposed for estimating the dispersion relation of waves propagating in an Euler-Bernoulli beam [14], and was further applied for estimating the loss factor of beam material [15] as well as the axial force of Timoshenko beam members [16]. The physical boundary conditions do not have to be modelled explicitly as their influence is accounted for in the estimated coefficients. However, this approach operates in the frequency domain and yields an estimate of the physical parameter for each frequency. Modelling errors and measurement noise can cause large fluctuation of the estimated values, requiring a proper interpretation prior to obtaining the final result. Moreover, the sag effect can no longer be disregarded when applying this method to long cables.

In order to tackle the above issues, a two-step methodology is proposed in the present work. In the first step, a segment of the cable, which is short enough to disregard the sag effect, is considered as a straight beam member modeled according to the Timoshenko beam theory. The axial force of this segment is then identified from the transverse responses, measured at a few locations of this segment. In the second step, the static state of the entire cable is considered, described by an analytical solution that gives the displacement, cable force and bending moment along the cable. The axial force in the segment, that was identified in the first step, is used as a reference, and the entire cable model is then updated. From this updated analytical model, the internal forces, including the axial force and bending moment, can be obtained at any location of the cable, providing more comprehensive information for the monitoring of the cable.

This paper consists of four parts: first, the dispersion relations of waves, governing the transverse motion of the cable, are studied, considering the influence of axial force and bending stiffness. Next, the numerical stability of the algorithm for estimating axial force is studied, and an iterative approach is developed to update the bending stiffness of the cable cross section. Afterwards, the analytical solution of the static state of cable is derived considering bending stiffness, sag effect as well as boundary conditions, and the method for updating the analytical model is proposed. Finally, numerical simulations, considering an inaccurate initial guess of the bending stiffness as well as measurement noise, are performed, proving the feasibility and potential of the proposed two-step methodology for the health monitoring of cable structures.

2. Step 1: estimation of the axial force of a cable segment

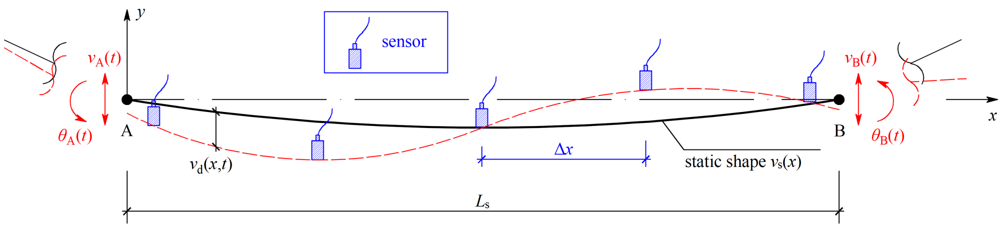

Figure 1: Transverse motion of a cable segment, measured by sensors spaced by Δx

In this part, a segment of cable (Fig. 1) is considered which is short enough for the sag effect to be negligible. The length of the segment should also not be too short, however, as it is the aim to identify, in the frequency range of interest, the wave components that constitute the cable response from measurements at a limited number of sensors [17]. The spacing between the sensors should therefore not be too small compared to the prevailing wavelengths. For this reason, a trade-off has to be made when choosing a proper value of L_s, and this will be discussed in detail later. In the following, the slip between cable wires is disregarded assuming that the wavelength is much larger than the dimension of the cross section [18]. In addition, the segment is assumed to be excited by an imposed motion at its boundaries, corresponding to the general case where a load (which does not need to be known) is applied at any location not on the segment. Taking into account shear deformation and rotational inertia, the equations of motion governing the transverse motion of the cable segment are written as: [13]:

$$\kappa GA(v_\mathrm{d}'' - \theta') + N_x v_\mathrm{d}'' - \rho A \ddot{v}_\mathrm{d} = 0 \tag{1}$$

$$EI\theta'' + \kappa GA(v_\mathrm{d}' - \theta') - \rho I \ddot{\theta} = 0 \tag{2}$$

with the boundary conditions:

$$v_\mathrm{d}|_{x=0}(t) = v_\mathrm{A}(t) \tag{3}$$

$$\theta|_{x=0}(t) = \theta_\mathrm{A}(t) \tag{4}$$

$$v_\mathrm{d}|_{x=L_\mathrm{s}}(t) = v_\mathrm{B}(t) \tag{5}$$

$$\theta|_{x=L_\mathrm{s}}(t) = \theta_\mathrm{B}(t) \tag{6}$$

where $v_\mathrm{d}(t)$ (m) and $\theta(t)$ (rad) are the transverse displacement and the rotation of cross section, respectively. The derivative of variables with respect to the spatial coordinate x and time t is denoted by a prime and a dot, respectively. The elastic and shear modulus of the cable are E (Pa) and G (Pa), respectively. The density of the cable material is ρ (kg/m^3). The area, the moment of inertia and the shear constant of the cross section are A (m^2), I (m^4) and κ (-), respectively. The axial force of the segment is N_x (N). The frequency-domain solution to Eqs. (1) and (2) takes the form of [13]:

$$\hat{V}(x,\omega) = \tilde{C}_1 \exp(k_1 x) + \tilde{C}_2 \exp[k_2(x - L_\mathrm{s})] + \tilde{C}_3 \exp(k_3 x) + \tilde{C}_4 \exp(k_4 x) \tag{7}$$

where $\tilde{C}_j$ ($j = 1, 2, 3, 4$) depend on the boundary conditions (Eqs. (3), (5), (4) and (6)), and k_1 up to k_4 are frequency dependent constants, satisfying the following dispersion relations:

$$k_1 = -\sqrt{\frac{-\beta + \sqrt{\beta^2 - 4\alpha\gamma}}{2\alpha}} \tag{8}$$

$$k_2 = \sqrt{\frac{-\beta + \sqrt{\beta^2 - 4\alpha\gamma}}{2\alpha}} \tag{9}$$

$$k_3 = -\sqrt{\frac{-\beta - \sqrt{\beta^2 - 4\alpha\gamma}}{2\alpha}} \tag{10}$$

$$k_4 = \sqrt{\frac{-\beta - \sqrt{\beta^2 - 4\alpha\gamma}}{2\alpha}} \tag{11}$$

where the coefficients α, β, γ are derived as follow:

$$\alpha = EI \cdot (\kappa GA + N_x) \tag{12}$$

$$\beta = -\kappa GAN_x - s^2 EI\rho A - s^2 \kappa GA\rho I - s^2 \rho IN_x \tag{13}$$

$$\gamma = s^2 \rho A \cdot (\kappa GA + s^2 \rho I) \tag{14}$$

where $s = \sigma + i\omega$ ($i = \sqrt{-1}$) is the complex frequency. The circular frequency is denoted by ω (Hz), and σ (-) can be taken zero for frequency-domain analysis, or a positive value in order to suppress the spectral leakage when time-domain response is involved [19]. For frequencies below the cut-off frequency ($\omega \le \omega_c = \sqrt{(\kappa GA)/(\rho I)}$), k_3 and k_4 are imaginary, corresponding to propagating wave components [17]. The phase velocities of these components are derived as:

$$c_{\mathrm{p}}(\omega) = \pm\omega\sqrt{\frac{2EI(N_x + \kappa GA)}{\sqrt{\Lambda^2 + 4\omega^2 EI\rho A(\kappa GA + N_x)(\kappa GA - \omega^2 \rho I)} + \Lambda}} \tag{15}$$

where

$$\Lambda = \omega^2 (EI\rho A + \kappa GA\rho I + N_{\mathrm{x}}\rho I) - \kappa GAN_x \tag{16}$$

The dispersion relations given by Eq. (15) are illustrated for a model of a cable consisting of 91 wires with a diameter of 7 mm. The material parameters are as follows: the elastic modulus $E = 200$ GPa, the density $\rho = 7800\ \mathrm{kg/m^3}$ and the Poisson ratio $\mu = 0.3$. The wires are assumed not to slip as mentioned before, so the geometric parameters are calculated for a solid cross section. Because of the irregular shape of the cross section, the geometric parameters are calculated using numerical integration, based on a discretization of the cross section, resulting in: the cross-section area $A = 0.0035\ \mathrm{m^2}$, the moment of inertia $I = 1.09 \times 10^{-6}\ \mathrm{m^4}$ and the shear constant $\kappa = 0.458$ [13]. The axial force is $N_x = 0.0035\ \mathrm{m^2} \times 100\ \mathrm{MPa} = 350$ kN, and the sag effect is disregarded. It is noted here that in a practical case, the axial force may change due to the external loads [20], and the bending stiffness may be different since the cross section may not be perfectly rigid as assumed for its estimation [18]. In order to investigate the effects of the cable force and the bending stiffness on the response of the cable, the axial force and the bending stiffness vary from $1.0N_x$ to $5.0N_x$ and from $0.5EI$ to $1.0EI$, respectively. The constants k_j ($j = 1, 2, 3, 4$) are then calculated by Eqs. (8), (9), (10) and (11), shown in Fig. 2.

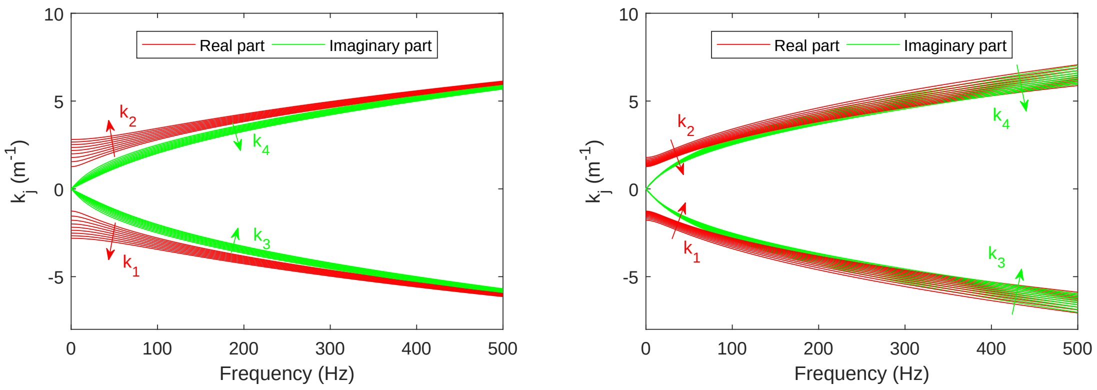

(a) (b)

Figure 2: Dispersion relation of the cable model with arrows denoting increasing values of the parameters: a) the axial force varies from $1.0N_x$ to $5.0N_x$; b) the bending stiffness varies from $0.5EI$ to $1.0EI$

By substituting the model parameters into Eq. (15), the phase velocities, which characterize the behavior of the propagating wave components, are calculated (Fig. 3). It is clear that the increase of either axial force or bending stiffness results in a higher phase velocity due to the increase in transverse stiffness. More importantly, the increase of the axial force results in a significant increase of the phase velocity in the lower frequency range (below 50 Hz in Fig. 3(a)), while the increase of the bending stiffness results in a significant increase of the phase velocity in the higher frequency range (above 400 Hz in Fig. 3(b)).

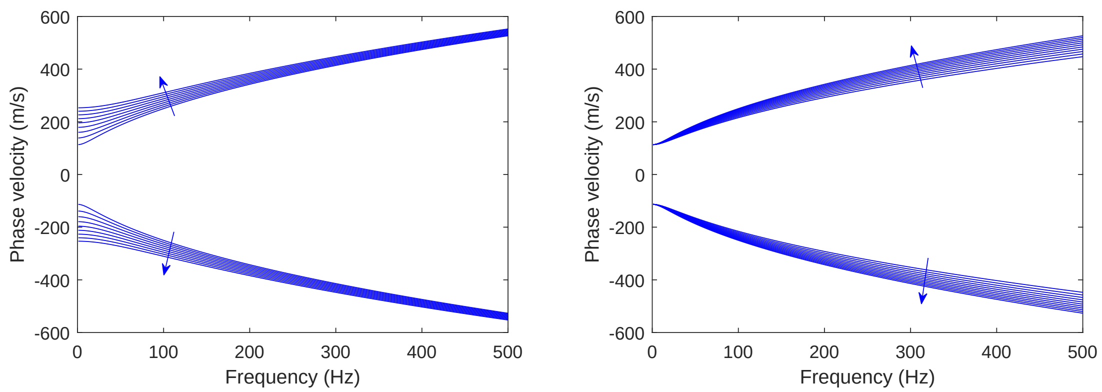

(a) (b)

Figure 3: Phase velocity of the cable model with arrows denoting increasing values of the parameters: a) the axial force varies from $1.0N_x$ to $5.0N_x$; b) the bending stiffness varies from $0.5EI$ to $1.0EI$

As shown in Fig. 1, m sensors, which are uniformly distributed with a spacing of Δx, are applied to measure the transverse response of the cable segment. Assuming that the measured responses provide exact samples of the analytical solution (Eq. (7)), the following matrix equation is obtained as:

$$\mathbf{H} \cdot \tilde{\mathbf{C}} = \hat{\mathbf{V}} \tag{17}$$

where

$$\mathbf{H}=\begin{bmatrix} 1 & \exp(-k_2L_\mathrm{s}) & 1 & 1 \\ \exp(k_1\Delta x) & \exp[k_2(\Delta x-L_\mathrm{s})] & \exp(k_3\Delta x) & \exp(k_4\Delta x) \\ \exp(2k_1\Delta x) & \exp[k_2(2\Delta x-L_\mathrm{s})] & \exp(2k_3\Delta x) & \exp(2k_4\Delta x) \\ \vdots & \vdots & \vdots & \vdots \\ \exp[(m-1)k_1\Delta x] & 1 & \exp[(m-1)k_3\Delta x] & \exp[(m-1)k_4\Delta x] \end{bmatrix}\in\mathbb{C}^{m\times 4} \quad (18)$$

is the characteristic matrix, representing the dynamic behavior of the cable segment.

$$\tilde{\mathbf{C}}=\left\{\tilde{C}_1 \quad \tilde{C}_2 \quad \tilde{C}_3 \quad \tilde{C}_4\right\}^\mathrm{T}\in\mathbb{C}^{4\times 1} \quad (19)$$

is the coefficient vector, which depends on the response at the boundaries of the cable segment.

$$\hat{\mathbf{V}}=\left\{\hat{V}_1 \quad \hat{V}_2 \quad \hat{V}_3\cdots\hat{V}_m\right\}^\mathrm{T}\in\mathbb{C}^{m\times 1} \quad (20)$$

is the vector containing the numerical Laplace transform [13] of the measured response. Since the matrix $\mathbf{H}$ can be calculated from the known parameters and $\hat{\mathbf{V}}$ can be obtained from the measurements, the remaining vector $\tilde{\mathbf{C}}$ can then be estimated by solving a linear least-squares problem:

$$\tilde{\mathbf{C}}^{(\mathrm{es})}=(\mathbf{H}^\mathrm{T}\mathbf{H})^{-1}\mathbf{H}^\mathrm{T}\hat{\mathbf{V}} \quad (21)$$

resulting in a fitting residual:

$$\boldsymbol{\varepsilon}=[\mathbf{H}(\mathbf{H}^\mathrm{T}\mathbf{H})^{-1}\mathbf{H}^\mathrm{T}-\mathbf{I}]\cdot\hat{\mathbf{V}} \quad (22)$$

when $m\geq 5$ [16]. For an arbitrary value assigned to the unknown axial force N_x, the fitting residual $\boldsymbol{\varepsilon}$ can be obtained from Eq. (22). The modulus of the fitting residual $\|\boldsymbol{\varepsilon}\|$ will be minimized when the value of N_x approximates the actual force in the cable segment:

$$N_x^{(\mathrm{es})}=\arg\min_{N_x}\frac{\|\boldsymbol{\varepsilon}\|^2}{\|\mathbf{H}(\mathbf{H}^\mathrm{T}\mathbf{H})^{-1}\mathbf{H}^\mathrm{T}\hat{\mathbf{V}}\|\cdot\|\hat{\mathbf{V}}\|} \quad (23)$$

When estimating the coefficient vector by Eq. (21), it is important to evaluate the numerical stability of the least-squares solution [21]. Assuming the measurements to be perturbed by $\delta\hat{\mathbf{V}}$, Eq. (17) becomes:

$$\mathbf{H}\cdot(\tilde{\mathbf{C}}+\delta\tilde{\mathbf{C}})=\hat{\mathbf{V}}+\delta\hat{\mathbf{V}} \quad (24)$$

The error of the estimated coefficient vector $\tilde{\mathbf{C}}$ is derived as:

$$\delta\tilde{\mathbf{C}}=(\mathbf{H}^\mathrm{T}\mathbf{H})^{-1}\mathbf{H}^\mathrm{T}\cdot\delta\hat{\mathbf{V}} \quad (25)$$

From the Cauchy–Schwarz inequality [22], we have:

$$\|\tilde{\mathbf{C}}\|\geq\frac{\|\mathbf{H}\cdot\tilde{\mathbf{C}}\|}{\|\mathbf{H}\|} \quad (26)$$

Also, the following inequality

$$\|\delta\tilde{\mathbf{C}}\|\leq\|(\mathbf{H}^\mathrm{T}\mathbf{H})^{-1}\mathbf{H}^\mathrm{T}\|\cdot\|\delta\hat{\mathbf{V}}\| \quad (27)$$

is obtained from Eq. (25). By dividing Eq. (27) by Eq. (26), the effect of the perturbation $\delta\hat{\mathbf{V}}$ on the estimated coefficient vector $\tilde{\mathbf{C}}^{(\mathrm{es})}$ is expressed as:

$$\frac{\|\delta\tilde{\mathbf{C}}\|}{\|\tilde{\mathbf{C}}\|}\leq\left[\|(\mathbf{H}^\mathrm{T}\mathbf{H})^{-1}\mathbf{H}^\mathrm{T}\|\cdot\|\mathbf{H}\|\cdot\frac{\|\hat{\mathbf{V}}\|}{\|\mathbf{H}\cdot\tilde{\mathbf{C}}\|}\right]\cdot\frac{\|\delta\hat{\mathbf{V}}\|}{\|\hat{\mathbf{V}}\|}\approx\mathrm{cond}(\mathbf{H})\cdot\frac{\|\delta\hat{\mathbf{V}}\|}{\|\hat{\mathbf{V}}\|} \quad (28)$$

Similarly, considering another perturbation of the matrix $\mathbf{H}$ in Eq. 18, i.e. $\delta\mathbf{H}$, for model imperfections such as the assumed constant axial force and the disregarded sag effect in the short segment when calculating the matrix $\mathbf{H}$ by Eq. (18). The resulting error of the estimated coefficient vector $\tilde{\mathbf{C}}^{(\mathrm{es})}$ is derived as:

$$\frac{\|\delta\tilde{\mathbf{C}}\|}{\|\tilde{\mathbf{C}}\|} \leq \mathrm{cond}(\mathbf{H}) \cdot \frac{\|\delta\mathbf{H}\|}{\|\mathbf{H}\|} \tag{29}$$

Both Eq. (28) and Eq. (29) imply that $\tilde{\mathbf{C}}^{(\mathrm{es})}$ may be significantly affected by model imperfections as well as measurement noise when the condition number of the matrix $\mathbf{H}$ is rather large, thus resulting in an inaccurate estimation of the axial force. Again, taking the model of the 91Φ7 cable as an example, the matrix $\mathbf{H}$ is evaluated by Eq. (18) in the frequency range $(0, 500]$ Hz and for a sensor spacing in the range $(0, 5]$ m. The resulting condition number of the matrix $\mathbf{H}$ is shown in Fig. 4.

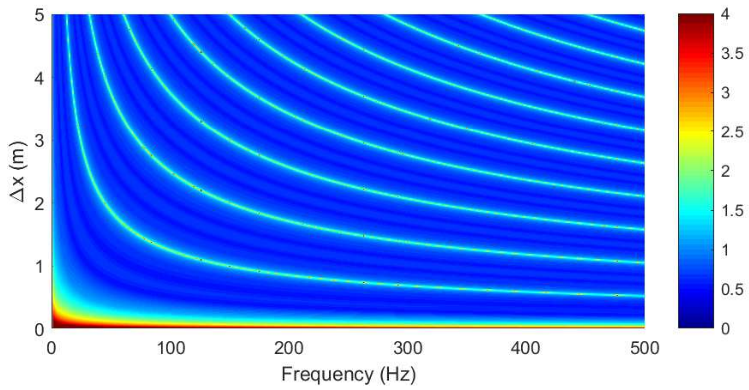

Figure 4: Logarithm of the condition number of the matrix $\mathbf{H}$ as a function of Δx and ω, i.e. $\log_{10}|\mathrm{cond}(\mathbf{H})|(\Delta x, \omega)$

As indicated before, the estimation of the axial force by Eq. (23) becomes inaccurate when the condition number of the matrix $\mathbf{H}$ is high. Fig. 5 illustrates the two cases in which the chosen sensor spacing results in a poor conditioning of the matrix $\mathbf{H}$.

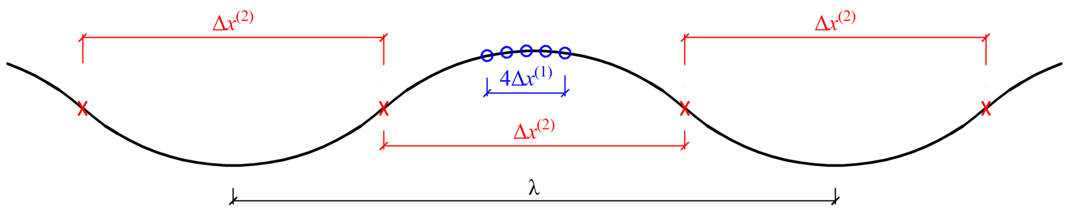

Figure 5: The sensor distribution leading to poor numerical stability (∘: $\Delta x^{(1)} \ll \lambda$. ×: $\Delta x^{(2)} \approx n\lambda/2,\ n = 1, 2, 3, \cdots$)

The red area at the bottom of Fig. 4 corresponds to the case where the sensors are distributed with a spacing $\Delta x^{(1)}$ that is small compared to the dominant wavelength governing the transverse cable response, while the light blue curves in Fig. 4 correspond to another case where the spacing $\Delta x^{(2)}$ corresponds to half a wavelength. For both cases, the measured responses are close to linearly dependent as they are either the same or have opposite signs, and this results in an inaccurate solution of Eq. (21). When determining the sensor distribution, the spacing Δx should be chosen carefully, considering the frequency range of excitation as well as the structural response, in order to avoid a poor conditioning of the estimation problem. In the process of data interpretation, the accuracy of the estimation can be verified by evaluating the condition number of the matrix $\mathbf{H}$.

When calculating the matrix $\mathbf{H}$ by Eq. (18), the bending stiffness of cable is usually difficult to quantify precisely because of the composite nature of the cross section [18]. For this reason, a joint estimation of the bending stiffness and the axial force is proposed next. Note that the vectors $\tilde{\mathbf{C}}$, $\hat{\mathbf{V}}$ and the matrix $\mathbf{H}$ are all frequency dependent, meaning that the axial force of the segment can be estimated independently at each frequency. Since the value of the axial force should be the same for each frequency, the linear term in the following fit to the estimated values should be zero:

$$N_x^{(\text{fit})}(\omega) = a_0 + a_1\omega \tag{30}$$

i.e., the factor a_1 of Eq. (30) should be zero. As indicated by Fig. 3, the influence of the axial force on the frequency response of the cable is more pronounced at lower frequencies, while the influence of the bending stiffness becomes more important at higher frequencies. From this, it can be deduced that an overestimation of the bending stiffness results in an underestimated axial force, and more importantly, this deviation increases with frequency, i.e. $\mathrm{d}N_x^{(\text{fit})}/\mathrm{d}\omega = a_1 < 0$, vice versa.

Taking $a_1 = 0$ as an objective, the bending stiffness can be updated by the Newton-Raphson's method until $\|a_1\|$ is sufficiently small, as shown in Fig. 6. Finally, the updated value $EI^{(\text{es})} = \eta EI$ is obtained, and the mean value of $N_x^{(\text{fit})}(\omega_j)$ $(j = 1, 2, \cdots, N)$ is calculated for a final value of the estimated axial force, that allows minimizing the influence from measurement noise $(\delta\hat{\mathbf{V}})$ and model imperfections $(\delta\mathbf{H})$. During this procedure, the values estimated at frequencies where the condition number of the matrix $\mathbf{H}$ is large should be considered as inaccurate and be rejected prior to the evaluation of Eq. (30).

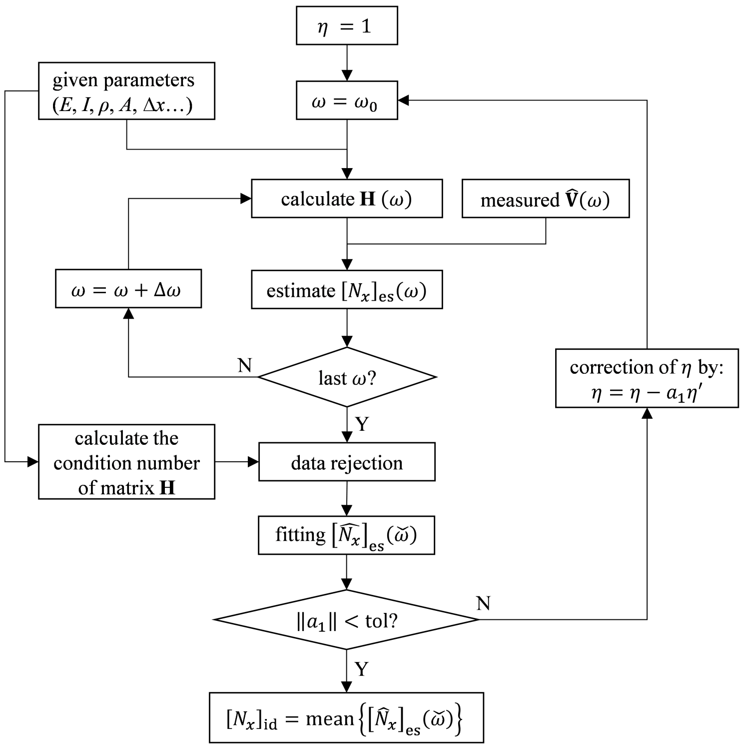

Figure 6: The flow chart for estimating the axial force N_x involving the determination of the updated bending stiffness ηEI

3. Step 2: updating of the static model of entire cable

In the second step, an analytical model describing the static state of the cable is used, taking into account the bending stiffness, the sag effect and the imposed rotations at the cable ends. This static model will be updated further by using the axial force at the location of the segment, that was identified in the first step.

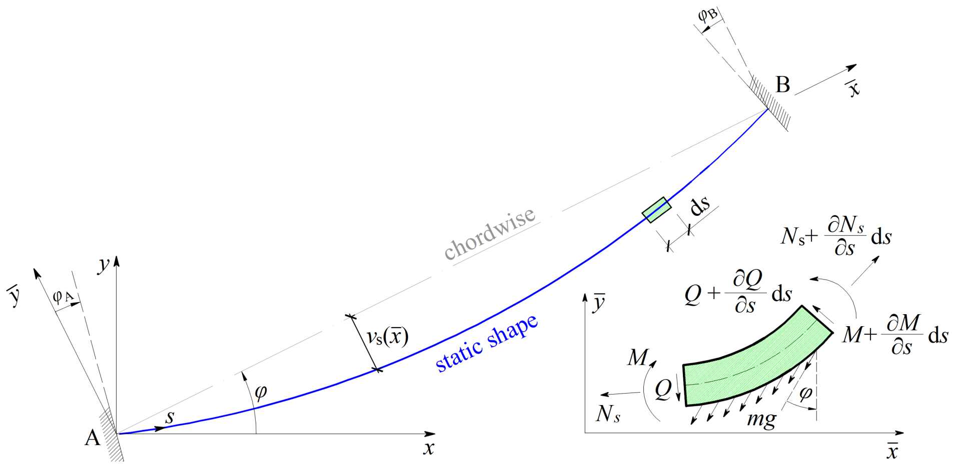

Figure 7: The static state of the entire cable model (by convention, a counter-clockwise direction is taken as positive for all angles in this study, such as φ_A, φ_B and φ.)

As shown in Fig. 7, a cable with an inclination φ (rad) is modelled in the global coordinate system xoy, where the gravity is along the y axis. Furthermore, the anchors may be either inclined or aligned with respect to the chord $o\bar{x}$. The angles φ_A and φ_B can be measured by means of an inclinator, providing the boundary conditions of the static model. For this model, the following assumptions are made:

- The length of the cable is much larger than the dimension of the cross section, so the shear deformation can be disregarded.
- The sag-span ratio is less than 1/8, therefore $\mathrm{d}s \approx \mathrm{d}\bar{x}$.
- The axial stiffness of the cable is much larger than its transverse stiffness, so the displacement component along the $\bar{x}$ axis can be disregarded.

For the differential segment $\mathrm{d}s$ of the cable, the equilibrium equations in the local coordinate system are formulated as follows:

$$\left(N_s + \frac{\partial N_s}{\partial s}\mathrm{d}s\right)\frac{\mathrm{d}\bar{x}}{\mathrm{d}s} - N_s\frac{\mathrm{d}\bar{x}}{\mathrm{d}s} - mg\sin\varphi\mathrm{d}s = 0 \tag{31}$$

$$\left(Q + \frac{\partial Q}{\partial s}\mathrm{d}s\right) - Q + \frac{\partial}{\partial s}\left(N_s\frac{\mathrm{d}v_s}{\mathrm{d}s}\right)\mathrm{d}s - mg\cos\varphi\mathrm{d}s = 0 \tag{32}$$

where N_s (N) and Q (N) are the axial force of the cable and the shear force of the cross section, respectively, which are both function of the location s. m (kg/m) is the mass of the cable per unit length, and g (N/kg) is the gravitational acceleration (normally $g = 9.8$ N/kg). The chordwise component (along the $\bar{x}$ direction) of the cable force is given as:

$$N_x = N_s\frac{\mathrm{d}\bar{x}}{\mathrm{d}s} \tag{33}$$

which is function of $\bar{x}$. By substituting Eq. (33) into Eq. (31), assuming $\mathrm{d}s \approx \mathrm{d}\bar{x}$, the chordwise component of the cable force is then expressed as:

$$\frac{\mathrm{d}N_x}{\mathrm{d}\bar{x}} - mg\sin\varphi = 0 \tag{34}$$

The integration of Eq. (34) along coordinate $\bar{x}$ yields:

$$N_x(\bar{x}) = N_{x0} + \bar{x}mg\sin\varphi \tag{35}$$

where the integration constant N_{x0} represents N_x at the location $\bar{x} = 0$. The relation between the shear force and the transverse displacement is [23]:

$$Q = -EI\frac{\mathrm{d}^3 v_\mathrm{s}}{\mathrm{d}\bar{x}^3} \tag{36}$$

By substituting Eq. (33), Eq. (35) and Eq. (36) into Eq. (32), the equilibrium equation in terms of the transverse displacement is formulated in the local coordinate system as follows:

$$-EI\frac{\mathrm{d}^4 v_\mathrm{s}}{\mathrm{d}\bar{x}^4} + (N_{x0} + \bar{x}mg\sin\varphi)\frac{\mathrm{d}^2 v_\mathrm{s}}{\mathrm{d}\bar{x}^2} + mg\sin\varphi\frac{\mathrm{d}v_\mathrm{s}}{\mathrm{d}\bar{x}} - mg\cos\varphi = 0 \tag{37}$$

Eq. (37) is rewritten in non-dimensional form as:

$$-\bar{\beta}\bar{v}_s^{(\mathrm{IV})} + (1 + \bar{\epsilon}\bar{\xi}\sin\varphi)\bar{v}_s^{(\mathrm{II})} + \bar{\epsilon}\sin\varphi\bar{v}_s^{(\mathrm{I})} - \cos\varphi = 0 \tag{38}$$

where a bracketed Roman number in superscript denotes the derivative to the non-dimensional spatial coordinate $\bar{\xi}$, and the non-dimensional parameters are defined as:

$$\bar{\beta} = (EI)/(N_{x0}L^2) \tag{39}$$

$$\bar{\epsilon} = mgL/N_{x0} \tag{40}$$

$$\bar{\xi} = \bar{x}/L \tag{41}$$

$$\bar{v}_s = v_\mathrm{s}N_{x0}/(mgL^2) \tag{42}$$

Eq. (38) is an ordinary differential equation of the fourth order with a variable coefficient for the term corresponding to $\bar{v}_s^{(\mathrm{II})}$, which cannot be solved analytically. In most cases, however, the cable force is much larger than the own weight of the cable, i.e., $N_{\mathrm{x}0} \gg mgL$, yielding $\bar{\epsilon} \approx 0$. Eq. (38) is therefore simplified to:

$$-\bar{\beta}\bar{v}_s^{(\mathrm{IV})} + \bar{v}_s^{(\mathrm{II})} - \cos\varphi = 0 \tag{43}$$

with the non-dimensional boundary conditions:

$$\bar{v}_s(0) = 0 \tag{44}$$

$$\bar{v}_s(1) = 0 \tag{45}$$

$$\bar{v}_s^{(\mathrm{I})}(0) = \bar{\varphi}_\mathrm{A} = \varphi_\mathrm{A}N_{x0}/(mgL) \tag{46}$$

$$\bar{v}_s^{(\mathrm{I})}(1) = \bar{\varphi}_\mathrm{B} = \varphi_\mathrm{B}N_{x0}/(mgL) \tag{47}$$

The complete solution to Eq. (43) is:

$$\bar{v}_s = C_1 + C_2\bar{\xi} + C_3\bar{\xi}^2 + C_4\exp\left(-\sqrt{1/\bar{\beta}}\bar{\xi}\right) + C_5\exp\left[\sqrt{1/\bar{\beta}}(\bar{\xi} - 1)\right] \tag{48}$$

where $C_3 = \cos\varphi/2$, and $C_3\bar{\xi}^2$ is therefore the particular solution. By substituting Eqs. (44), (45), (46) and (47) into Eq. (48), a matrix equation is obtained:

$$\begin{bmatrix} 1 & 0 & 1 & \exp(-\bar{\gamma}) \\ 1 & 1 & \exp(-\bar{\gamma}) & 1 \\ 0 & 1 & -\bar{\gamma} & \bar{\gamma}\exp(-\bar{\gamma}) \\ 0 & 1 & -\bar{\gamma}\exp(-\bar{\gamma}) & \bar{\gamma} \end{bmatrix} \begin{Bmatrix} C_1 \\ C_2 \\ C_4 \\ C_5 \end{Bmatrix} = \begin{Bmatrix} 0 \\ -\cos\varphi/2 \\ \bar{\varphi}_\mathrm{A} \\ \bar{\varphi}_\mathrm{B} - \cos\varphi \end{Bmatrix} \tag{49}$$

where

$$\bar{\gamma} = \sqrt{1/\bar{\beta}} \tag{50}$$

From Eq. (49), the constants C_1, C_2, C_4, C_5 are obtained, and the static shape can be evaluated by Eq. (48). By substituting Eqs. (39), (40), (41) and (42) into Eq. (48), the rotation of the cross section is found:

$$\frac{\mathrm{d}v_\mathrm{s}}{\mathrm{d}\bar{x}} = \frac{mg}{N_{x0}}\left\{C_2L + \bar{x}\cos\varphi - C_4\bar{\gamma}L\exp\left(-\frac{\bar{\gamma}\bar{x}}{L}\right) + C_5\bar{\gamma}L\exp\left[\bar{\gamma}\left(\frac{\bar{x}}{L} - 1\right)\right]\right\} \tag{51}$$

Similarly, the curvature is found as the second derivative of the transverse displacement:

$$\frac{\mathrm{d}^2 v_\mathrm{s}}{\mathrm{d}\bar{x}^2} = \frac{mg}{N_{x0}} \left\{ \cos\varphi + C_4\bar{\gamma}^2 \exp\left(-\frac{\bar{\gamma}\bar{x}}{L}\right) + C_5\bar{\gamma}^2 \exp\left[\bar{\gamma}\left(\frac{\bar{x}}{L} - 1\right)\right] \right\} \tag{52}$$

Therefore, the axial force and the moment of the cable, which are function of $\bar{x}$, are evaluated by:

$$N_\mathrm{s}(\bar{x}) = N_x \cdot \frac{\mathrm{d}s}{\mathrm{d}\bar{x}} = (N_{x0} + \bar{x}mg\sin\varphi) \cdot \sqrt{1 + \left(\frac{\mathrm{d}v_\mathrm{s}}{\mathrm{d}\bar{x}}\right)^2} \tag{53}$$

$$M(\bar{x}) = -EI \cdot \frac{\mathrm{d}^2 v_\mathrm{s}}{\mathrm{d}\bar{x}^2} \tag{54}$$

From the first step, the axial force at the location of the segment as well as the bending stiffness of the cross section have been obtained. The angles of the boundaries φ_A and φ_B can be obtained by measuring the inclinations of the anchors as mentioned before. Based on the above, only the parameter N_{x0} remains unknown for Eq. (53) and Eq. (54). Note that there is a one-to-one correspondence between N_{x0} and the axial force at the location of the segment $N_x(\bar{x}_\mathrm{s})$, and such relation is continuous and smooth. N_{x0} can therefore be updated by the bi-section method, ensuring that $N_x(x_\mathrm{s})$ approximates the value $\hat{N}_x^{(\mathrm{es})}$ identified in the first step. Afterwards, the internal force at arbitrary location of the cable is found from the updated static model of the entire cable (Eq. (48), Eq. (53) and Eq. (54)).

4. Feasibility study - numerical simulation

In the case of a slack cable which has a relatively small cable force, the application of existing methods, such as the widely used taut string theory [8], leads to inaccurate estimations of the cable force, due to the inappropriate simplifications (e.g. disregarding the sag effect and bending stiffness, perfect boundary conditions). This may be the case during construction or when damage in the cable resulting in a loss of prestress. In order to demonstrate the applicability of the two-step methodology in such a case, a cable with a small initial strain is considered in this section. All the numerical simulations are performed using the two-step FEM-SEM approach proposed in [13].

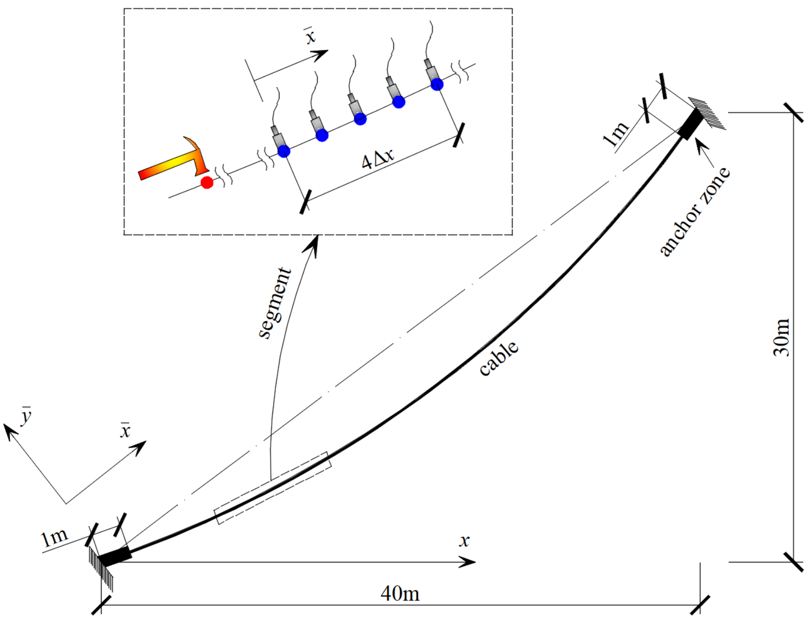

Figure 8: Cable model considered in the numerical simulation of the test

For the cable model shown in Fig. 8, the material and geometric parameters have been given in Section 2. In this example, the moment of inertia is reduced by 80% as $I_{\mathrm{zz}} = 0.80 \times 1.09 \times 10^{-6}\ \mathrm{m}^4 = 0.87 \times 10^{-6}\ \mathrm{m}^4$, and the initial strain of the cable is given a value $\varepsilon_0 = 5 \times 10^{-4}$. Additionally, at both ends of the cable, the anchor zones are simulated by segments with a bending stiffness which is 10 times larger than the one of the cable. A concentrated mass of 30 g is considered at the location of each measurement point, representing the mass of the sensor. From the finite element analysis, the static configuration of the cable is obtained, including the static displacements and internal forces. Note that the rotational angles of both anchors are close to zero ($\varphi_{\mathrm{A}} = -0.0016$ rad, $\varphi_{\mathrm{B}} = 0.0016$ rad) due to the large bending stiffness of the anchor zones. Therefore, $\varphi_{\mathrm{A}} = \varphi_{\mathrm{B}} = 0$ rad will be considered as known parameters in the analysis following next.

The segment where $\bar{x} \in [6, 10]$ m is defined for the estimation of axial force in the first step, as shown in Fig. 8. The excitation is modelled as a linear impact at the location $\bar{x} = 5$ m, which is not on the segment. The cable is assumed to be very lightly damped, and the damping force is proportional to the velocity of transverse motion with the damping coefficient $c_{\mathrm{t}} = 0.226\ \mathrm{N \cdot s/m}$. The time-domain signal and the frequency spectrum of the impact are shown in Fig. 9.

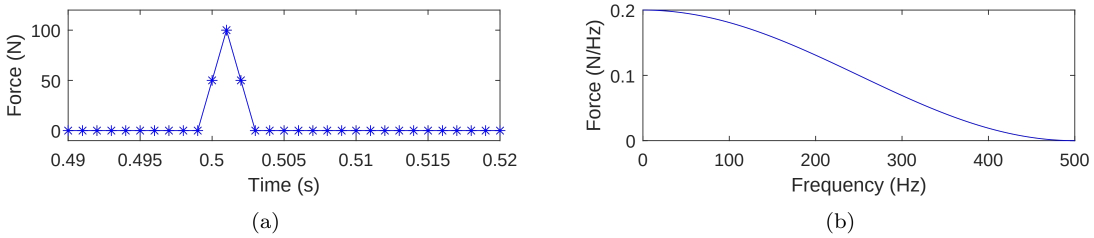

Figure 9: Hammer impact: a) time-domain signal b) frequency spectrum

Based on the static state, the dynamic response of the model is simulated by means of the spectral element method, yielding the acceleration responses at the sensor locations $\bar{\mathbf{x}} = \{6\ 7\ 8\ 9\ 10\}^{\mathrm{T}}$ (Fig. 10).

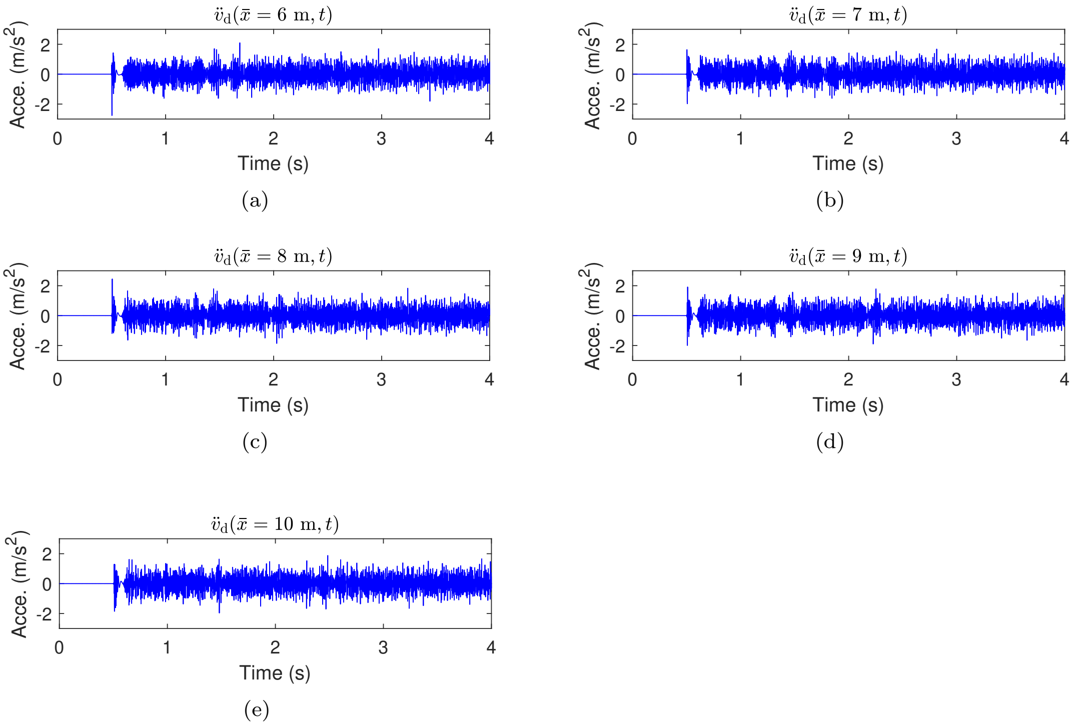

Figure 10: Acceleration response of the cable: a) $\bar{x} = 6$ m b) $\bar{x} = 7$ m c) $\bar{x} = 8$ m d) $\bar{x} = 9$ m e) $\bar{x} = 10$ m

As an initial guess in the analysis, a value of $EI = \eta \cdot EI_0 = 1.00 \times 1.09 \times 10^{-6}$ m^4 is taken for the bending stiffness. By substituting the Laplace transform of the measured responses (as shown in Fig. 10) into Eq. (22), fitting residuals are evaluated for values of the axial force between -1500 kN and 1500 kN, considering a step size of 1 kN. At each frequency ω_j, an axial force $N_x^{(\mathrm{es})}(\omega_j)$ is estimated by searching the minimum of the fitting residual (Eq. (23)) over the span of axial forces, shown in Fig. 11.

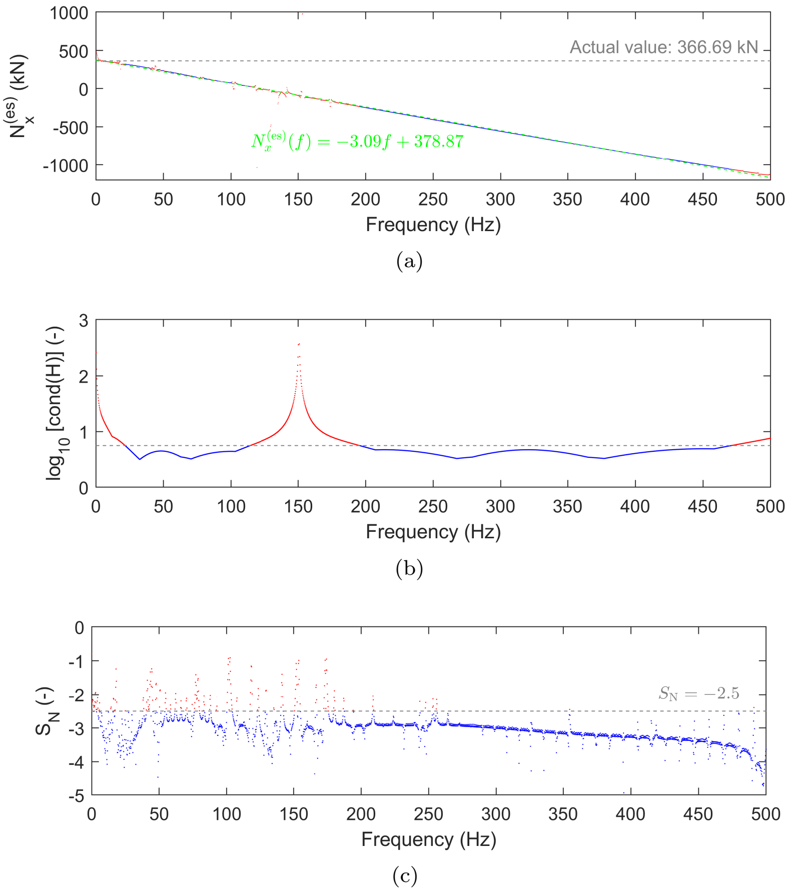

Figure 11: Identification of the axial force where η = 1.00 for the initial guess (The blue dots and red dots denote the frequency points where the estimated axial forces are accurate and inaccurate, respectively): a) estimated axial force $N_x^{(\mathrm{es})}(\omega_j)$ b) condition number of the matrix $\mathbf{H}$ c) indicator of sensitivity $S_{\mathrm{N}}(\omega_j)$

In Fig. 11(a), it is clear that the data points $N_x^{\mathrm{es}}(\omega_j)$ $(j = 1, 2, \cdots, N)$ follow a downward linear trend as a function of frequency. It can be seen that the estimated axial force even becomes negative when the fitting residual $\|\varepsilon\|$ (Eq. (22)) is minimized, and this trend implies that the bending stiffness is largely overestimated. Moreover, note that small deviations from this trend can be observed in the frequency ranges $f \in (0, 10) \cup (130, 170) \cup (460, 500)$ Hz, which is caused by the following model imperfections:

- The masses of the sensors are considered in the numerical simulations of the experiment, but disregarded in the estimation of the axial force, as Eq. 7 is the response of cable with a uniformly distributed mass.
- In the numerical simulation of the experiment, the cable is assumed to be lightly damped, while damping is disregarded when estimating the axial force by Eq. (23).
- Due to the inclination and the sag of the segment, the axial force N_x should in principle depend on x, but this dependency is disregarded for the short segment considered when applying Eq. (1).

Although these effects are quite small, they are significantly amplified in the estimation of the axial force when the condition number of the matrix $\mathbf{H}$ (Fig. 11(b)) is high, leading to the fluctuations observed in Fig. 11(a). In order to further improve the robustness of the estimation of the axial force, an additional criterion is defined as:

$$S_{\mathrm{N}}(\omega_j) = \log_{10}\left|\frac{\varepsilon(N_x^{(\mathrm{es})};\omega_j)}{\frac{1}{M}\sum_{n=1}^{M}\varepsilon(N_x(n);\omega_j)}\right| \quad (j = 1, 2, \cdots, N) \tag{55}$$

which represents the sensitivity of the fitting residual (ε of Eq. (23)) to the axial force N_x at the frequency ω_j, shown in Fig. 11(c). The numerator in Eq. (55) is the minimized fitting residual for the selected axial force, while the denominator in Eq. (55) is the average value of the fitting residuals over the whole span of the axial forces $N_x(n)$ $(n = 1, 2, \cdots, M)$. Therefore, small values of S_{N} correspond to an accurate estimation of $N_x^{(\mathrm{es})}$, as the fitting residuals are sensitive to the axial force. In order to reject inaccurate estimations of the axial force, in this procedure, a threshold is set on the condition number of the matrix $\mathbf{H}$ as well as on the indicator of sensitivity S_{N}. This entails a trade-off between the accuracy and the volume of selected data. In this case, a threshold of $\{N_x^{(\mathrm{es})}(\omega_j) | \log_{10}|\mathrm{cond}(\mathbf{H})(\omega_j)| < 0.75 || S_{\mathrm{N}}(\omega_j) < -2.5\}$ has been used to select the values of the axial forces which are considered accurate. Next, a linear trend is fitted (Fig. 11(a)) to the selected data points which are considered as accurate. The factor of the bending stiffness η is then updated iteratively following the process in Fig. 6 until $\|a_1\| \to 0$.

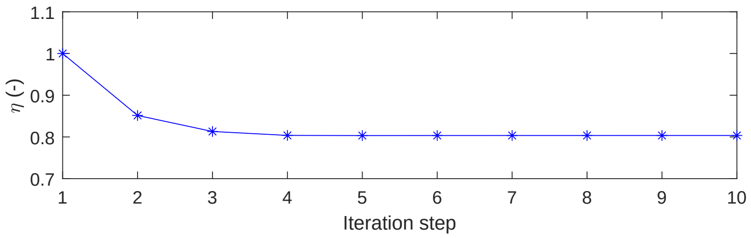

Figure 12: The updating of the bending stiffness factor η (starting from $\eta = 1.00$)

After a few iterations, the bending stiffness factor η converges to a value of 0.80, which equals the correct value, as shown in Fig. 12. The estimated data points of $N_x^{(\mathrm{es})}(\omega_j)$ are distributed along a straight horizontal line (Fig. 13(a)), showing that the estimated axial force is now independent of frequency.

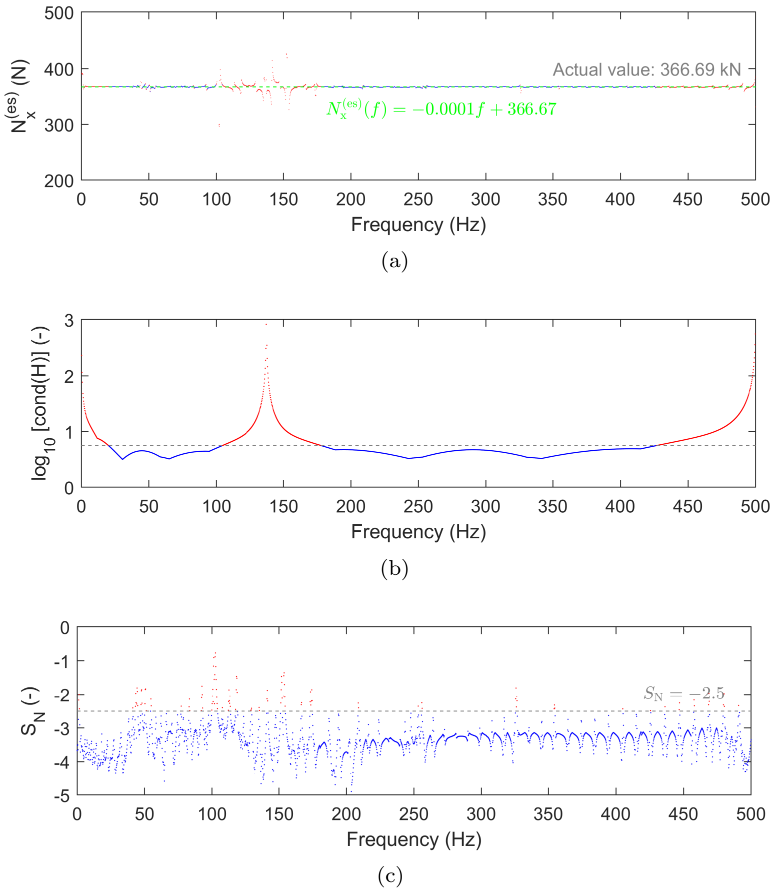

Figure 13: Identification of the axial force where $\eta = 0.80$ for the convergency (The blue dots and red dots denote the frequency points where the estimated axial forces are accurate and inaccurate, respectively): a) estimated axial force $N_x^{(es)}(\omega_j)$ b) condition number of the matrix $\mathbf{H}$ c) indicator of sensitivity $S_{\mathrm{N}}(\omega_j)$

By calculating the average value of the selected data in Fig. 13(a), the slight fluctuations are eliminated, and the axial force is finally identified as 366.64 kN, which is quite close to the reference value of the FE model (366.69 kN). By comparing Fig. 13(b) with Fig. 11(b), it can be concluded that the condition number of the matrix $\mathbf{H}$ is not too sensitive to the bending stiffness. For rather small changes in bending stiffness, it may not be necessary to update the condition number of the matrix $\mathbf{H}$, allowing for a reduction of the computational cost. As a reference, the cable force is also estimated from the first natural frequency of the cable (1.27 Hz), using conventional methods including the taut string theory [8] and the improved empirical equation [11]. The results are shown in Tab. 1.

Table 1: Comparison of the cable forces identified by the existing methods and the proposed method

Method	Formula	Effective length	Bending stiffness	Axial force	Error
Taut string [8]	$\hat{N}_x = 4mL^2 f_n^2/n^2$	48 m	–	406.03 kN	10.73%
Empirical [11]	$\hat{N}_x = m\left(2Lf - \frac{2.363}{L}\sqrt{\frac{EI}{\rho A}}\right)^2$	48 m	$\eta = 0.80$ (known)	380.25 kN	3.70%
This paper	$\hat{N}_x = \sum_{j=1}^{N} N_x^{(es)}(\omega_j)/N$	–	$\eta = 1.00$ (guess)	366.64 kN	-0.01%

The cable force identified by the taut string theory is much larger than the true value, because both the bending stiffness and the sag effect are disregarded, and, moreover, the effective cable length is difficult to determine for the anchor zones which extend over a length of 1 m at both ends. For the empirical equation proposed in [11], the accuracy of the estimation is significantly improved by taking into consideration the effect of bending stiffness. However, an error 3.70% remains present, caused by the unclear definition of the effective cable length when considering the anchor zones. For the method proposed in this paper, the bending stiffness is taken into account, and the boundary conditions implicitly involved in the coefficient vector $\mathbf{C}$ (Eq. (19)) have no effect on the estimation of the axial force. The effects of model imperfections, such as the disregarded sag effect and the damping in the cable, will lead to a perturbation $\delta\mathbf{H}$ of Eq. 29, but an amplification of these errors is avoided by adopting the threshold for the condition number of the matrix $\mathbf{H}$. This leads to a significant improvement of the accuracy of the axial force estimation.

In order to study the effect of measurement noise on the estimated axial force, the acceleration responses are further polluted by white noise, and multiple signal noise ratios (SNR) are considered by changing the amplitude of the noise. For each case, the axial force is identified similarly as above. After data rejection, the ratio (R_{N}) of the number of remaining data points and the total number of data points, is calculated, giving an indication of the volume of useful information involved in the measured response.

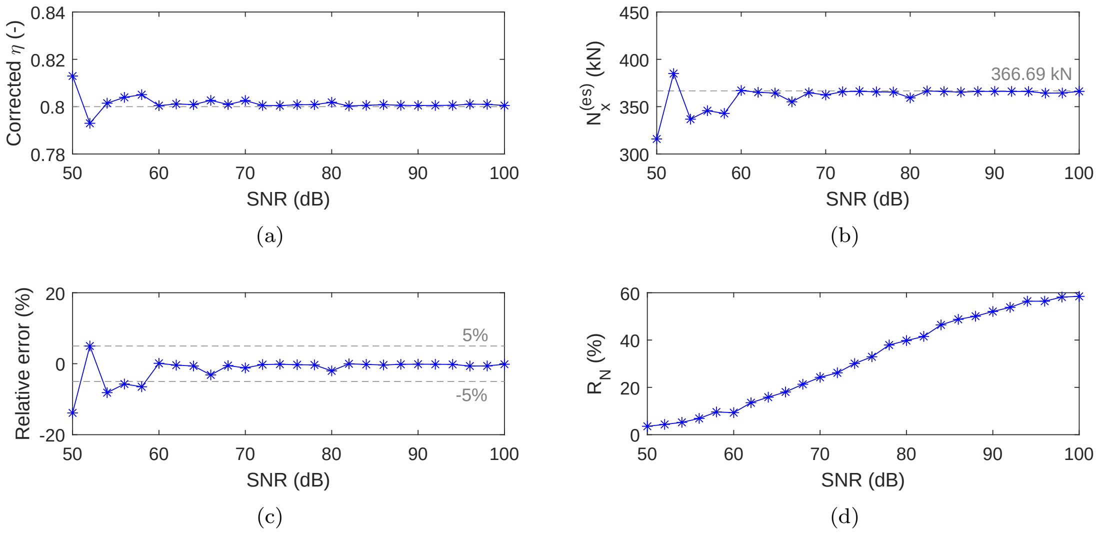

Figure 14: Identification of the axial force with increasing measurement noise: a) update of the bending stiffness factor b) identification of the axial force c) relative error d) volume of the useful information

Figs. 14(a), 14(b) and 14(c) show that both the bending stiffness and the axial force can be identified correctly, with the relative error of the identified axial force not exceeding 3%, as long as the SNR is higher than 60 dB. The data significantly affected by noise are rejected, as evidenced by Fig. 14(d). When the SNR is lower than 60 dB, the ratio of useful information is less than 10%, which is insufficient to obtain a reliable result. In the present case, the proposed methodology leads to a reliable identification of the axial force when SNR is higher than 60 dB.

Based on the identified axial force of the segment, the parameter N_{x0}, involved in the analytical static solution in Eqs. (48), (53) and (54), is updated by means of the bi-section method, giving a value of the updated parameter $N_{x0} = 365.39$ kN. From this updated static model, the static shape, the distributed axial force and the bending moment of the cable can now be evaluated. The above results are compared with those directly obtained from the finite element model for a validation, shown in Fig. 15.

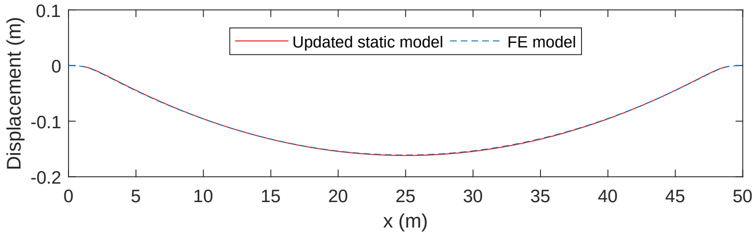

(a)

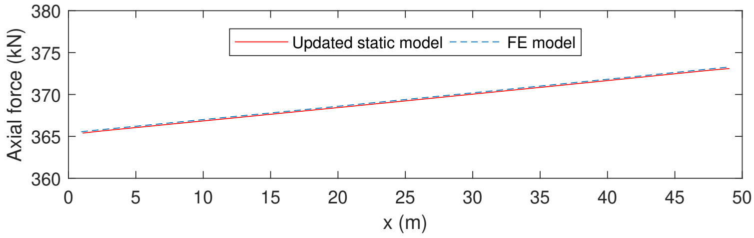

(b)

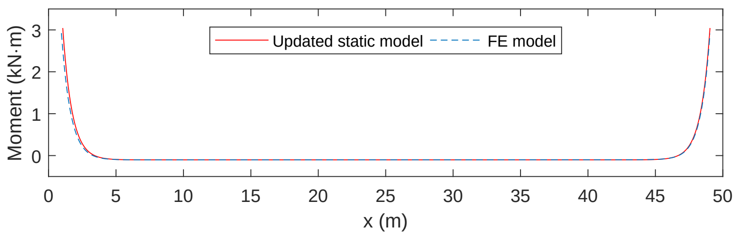

(c)

Figure 15: Comparison between the updated analytical model and the FE model of the cable: a) displacement b) cable force c) bending moment

The comparison shows that the static displacement, the cable force and bending moment, evaluated from the updated static model of the entire cable, all agree well with those of the actual cable (i.e. the FE model in Fig. 15). These results also allow for an estimation of the maximum stress, appearing at the top anchor of the cable, given as:

$$\sigma = \sigma_{N_x} + \sigma_{\mathrm{M}} = \frac{N_x}{A} + \frac{M}{I_{\mathrm{zz}}} \cdot \frac{D}{2} = \frac{372.98 \text{ kN}}{0.0035 \text{ m}^2} + \frac{3.045 \text{ kN} \cdot \text{m}}{0.8 \times 1.09 \times 10^{-6} \text{ m}^4} \cdot \frac{0.077 \text{ m}}{2} = 241.01 \text{ MPa} \tag{56}$$

where $\sigma_{\mathrm{M}} = 134.44$ MPa is the bending stress of the cable. Note that it is difficult in practice, in particular for existing structures, to estimate the bending stress of cables, although it is important for the evaluation of fatigue life.

5. Conclusion

In the present work, a two-step methodology is proposed for the identification of cable force. First, the axial force of a cable segment with limited length is identified considering the updating of bending stiffness. During this step, the physical boundaries of cable do not need to be known, while the sag effect is disregarded for this short segment. By considering the identified axial force as a known parameter, the static model of the entire cable is updated next, allowing the evaluation of the cable force and bending moment along the cable. Compared to the existing techniques, the proposed methodology has the following advantages:

- The boundary conditions of the segment are implicitly involved in the coefficients to be estimated, and do not have to be modelled based on physical grounds. The identification of axial force is hardly affected by the sag effect as the segment is taken sufficiently short.
- The bending stiffness of the cable can be updated during the identification of axial force, so an appropriate value can be obtained even for an inaccurate initial guess on the bending stiffness.
- The numerical stability of the estimation procedure is evaluated by means of an indicator which is based on the condition number of the characteristic matrix. The proposed data rejection improves the robustness against model imperfections (such as the damping, sag effect and inclination of the segment) as well as measurement noise.
- The updated static model can be used to compute the axial force and bending moment along the cable, allowing for an evaluation of the stresses, especially for the additional stress resulting from the bending deformation.

Acknowledgment

The first author was an international scholar in the Department of Civil Engineering, KU Leuven, supported by the China Scholarship Council (CSC) during the early stage of this study. The financial support is gratefully acknowledged.

References

References

[1] J. Y. Zhang, M. Ohsaki, Force identification of prestressed pin-jointed structures, Computers and Structures 89 (23) (2011) 2361–2368.
[2] D. Degrauwe, G. De Roeck, G. Lombaert, Uncertainty quantification in the damage assessment of a cable-stayed bridge by means of fuzzy numbers, Computers & Structures 87 (17–18) (2009) 1077–1084.
[3] A. B. Mehrabi, In-service evaluation of cable-stayed bridges, overview of available methods and findings, Journal of Bridge Engineering 11 (6) (2006) 716–724.
[4] S. E. H. A. M. Zarbaf, M. Norouzi, R. J. Allemang, V. J. Hunt, A. Helmicki, D. K. Nims, Stay force estimation in cable-stayed bridges using stochastic subspace identification methods, Journal of Bridge Engineering 22 (9) (2017) 0001091.
[5] S. Li, E. Reynders, K. Maes, G. De Roeck, Vibration-based estimation of axial force for a beam member with uncertain boundary conditions, Journal of Sound and Vibration 332 (4) (2013) 795–806.
[6] A. B. Mehrabi, S. Farhangdoust, A laser-based noncontact vibration technique for health monitoring of structural cables: background, success, and new developments, Advances in Acoustics and Vibration (2018) 8640674.
[7] B. Peeters, G. De Roeck, Stochastic system identification for operational modal analysis: a review, Journal of Dynamic Systems, Measurement, and Control 123 (4) (2001) 659–667.
[8] H. M. Irvine, Cable structures, New York: ASCE Press, 1992.
[9] J. Humar, Dynamics of Structures: Second Edition, Crc Press, 2002.
[10] R. Geier, G. De Roeck, R. Flesch, Accurate cable force determination using ambient vibration measurements, Structure & Infrastructure Engineering 2 (1) (2006) 43–52.
[11] W. X. Ren, G. Chen, W. H. Hu, Empirical formulas to estimate cable tension by cable fundamental frequency, Structural Engineering and Mechanics 20 (3) (2005) 363–380.
[12] B. F. Yan, J. Yu, M. Soliman, Estimation of cable tension force independent of complex boundary conditions, Journal of Engineering Mechanics 141 (1) (2015) 06014015.
[13] S. H. Zhang, R. L. Shen, T. Wang, G. De Roeck, G. Lombaert, A two-step FEM-SEM approach for wave propagation analysis in cable structures, Journal of Sound and Vibration 415 (2018) 41–58.
[14] J. G. Mcdaniel, W. S. S. Jr, Estimation of structural wave numbers from spatially sparse response measurements, Journal of the Acoustical Society of America 108 (4) (2000) 1674–1682.
[15] Y. B. Liao, V. Wells, Estimation of complex modulus using wave coefficients, Journal of Sound and Vibration 295 (2006) 165–193.
[16] K. Maes, J. Peeters, E. Reynders, G. Lombaert, G. De Roeck, Identification of axial forces in beam members by local vibration measurements, Journal of Sound and Vibration 332 (21) (2013) 5417–5432.
[17] S. H. Zhang, R. L. Shen, K. S. Dai, L. Wang, G. De Roeck, G. Lombaert, A methodology for cable damage identification based on wave decomposition, Journal of Sound and Vibration 442 (2019) 527–551.
[18] K. Spak, G. Agnes, D. Inman, Parameters for modeling stranded cables as structural beams, Experimental Mechanics 54 (9) (2014) 1613–1626.

[19] D. Wilcox, Numerical Laplace transformation and inversion, International Journal of Electrical Engineering Education 15 (3) (1978) 247–265.
[20] S. L. Li, S. Y. Wei, Y. Q. Bao, H. Li, Condition assessment of cables by pattern recognition of vehicle-induced cable tension ratio, Engineering Structures 155 (2018) 1–15.
[21] W. Cheney, D. Kincaid, Numerical mathematics and computing, Belmont: Brooks Cole, 2012.
[22] G. Golub, C. F. Van Loan, Matrix computations, Baltimore: The Johns Hopkins University Press, 1996.
[23] W. Weaver Jr, S. P. Timoshenko, D. H. Young, Vibration problems in engineering, John Wiley & Sons, New York, 1990.